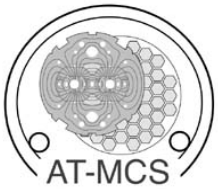

Magnets, Cryostats and Superconductors
AT-MCS

February 2008
EDMS no: 890590

LHC Project Note 409

Assessment of Static Heat Loads in the LHC Arc, from the Commissioning of Sector 7-8

C. Maglioni, V. Parma

Summary

This note presents first estimates of the static heat loads in the LHC arc cryostats, evaluated experimentally during the commissioning of sector 7-8 in April 2007.
Heat loads to the thermal shielding are estimated from the non-isothermal cooling of the supercritical helium in line *E*, while heat loads to the 1.9K level of the cold masses are estimated from the internal energy balance during a natural warm-up of the sector in the absence of active cooling.
A comparison of the measured heat loads with the budgeted heat loads is then presented and discussed.

1. INTRODUCTION

Assuming as fundamental background and reference the thermal performance highlighted by the various thermal models, experimental setups and strings tested at CERN ([4] and [5]), the recent commissioning of sector 7-8 provided the first possibility to validate this performance on a full sector scale.
The first part of this work presents the evaluation of the helium mass flow inside the thermal shield cooling line (header *E*) and the assessment of the profile of the thermal shield static heat load along the sector layout. Then, the second part concerns the assessment of the static heat loads to the cold masses at 1.9K.
The two assessments require different approaches, which must therefore be based upon different time periods and data acquisitions. The results are discussed and compared to the respective budgeted heat loads, extrapolated from [3].

2. THERMAL SHIELD STATIC HEAT LOAD

The heat load to the thermal shield was estimated as the enthalpy balance of the non-isothermal heating of supercritical helium along line *E*.
The thermal shield receives heat mainly by radiation from the vacuum vessel and by conduction through different heat intercepts (support posts mainly and also DCF, beam tubes pumping manifolds, etc..), as schematically shown in Figure 1.

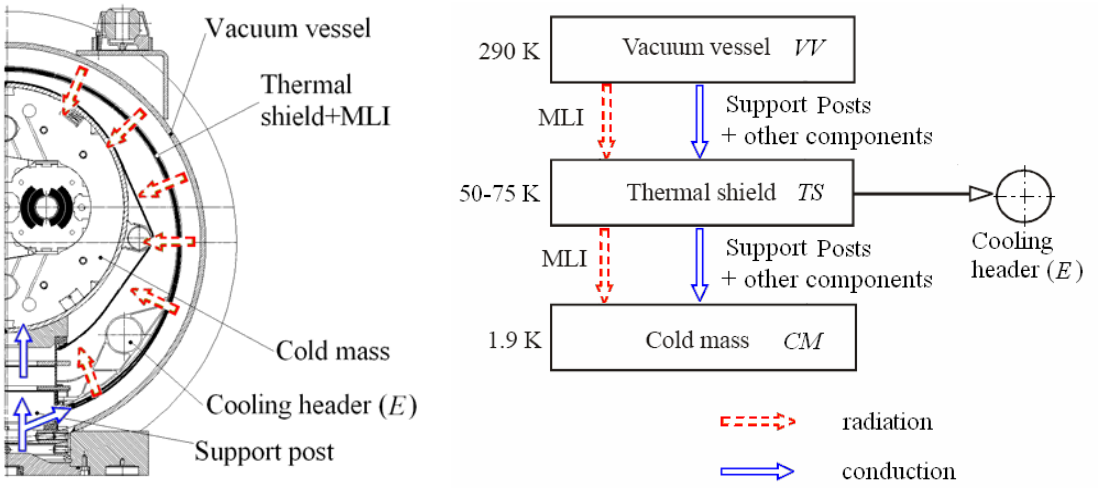

Figure 1 – Scheme of the main thermal flow of a cryostat

Therefore, estimating the helium enthalpy balance inside the thermal shield cooling line results in a net load, which is the difference between the heat received by the shield and the heat leaving to the cold mass:

$$W_E = W_{VV \to TS} - W_{TS \to CM} \qquad [\mathrm{W}] \qquad (1)$$

In the following, when referring to *thermal shield heat loads*, the meaning is therefore *net static heat load adsorbed by header E*.
Data were taken from Timber-SCADA interface, during a period of three days with one minute frequency[1]. The sensors used are listed in Table 1.

[1] SCADA is the Supervisory Control And Data Acquisition system. The chosen period lasted from 18:00 of 6th to 18:00 of 9th, April 2007. The acquisition was made in scale down repeat mode.

Table 1 – Sensors for thermal shield heat load evaluation in sector 7-8

Sensor	Reading	Location	Description
TT901	T [K]	LSS L8 before DFBAO	Line *E* supply temperature
TT801	T [K]	L8, R7 quadrupole service module (DS & ARC) approximately one every two phase separator	Line *E* temperature
PT700	p [bar]	Point 8 QUICC	Line *E* input pressure
PT981	p [bar]	QRL return module before CV988	Line *E* output pressure

The period chosen was the most representative compromise between nominal and stable equilibrium conditions for the thermal shield. Moreover both cold masses and line *C'* were in nominal and stable conditions during this period. Supply temperature of header *E* (T_{supply}) was stable since a few days, with variations of less than 4% around the mean value, and also during the entire chosen period. Its value, however, was lower than nominal (44.6 ± 0.8K instead of 50K), as can be clearly seen from Figure 2.

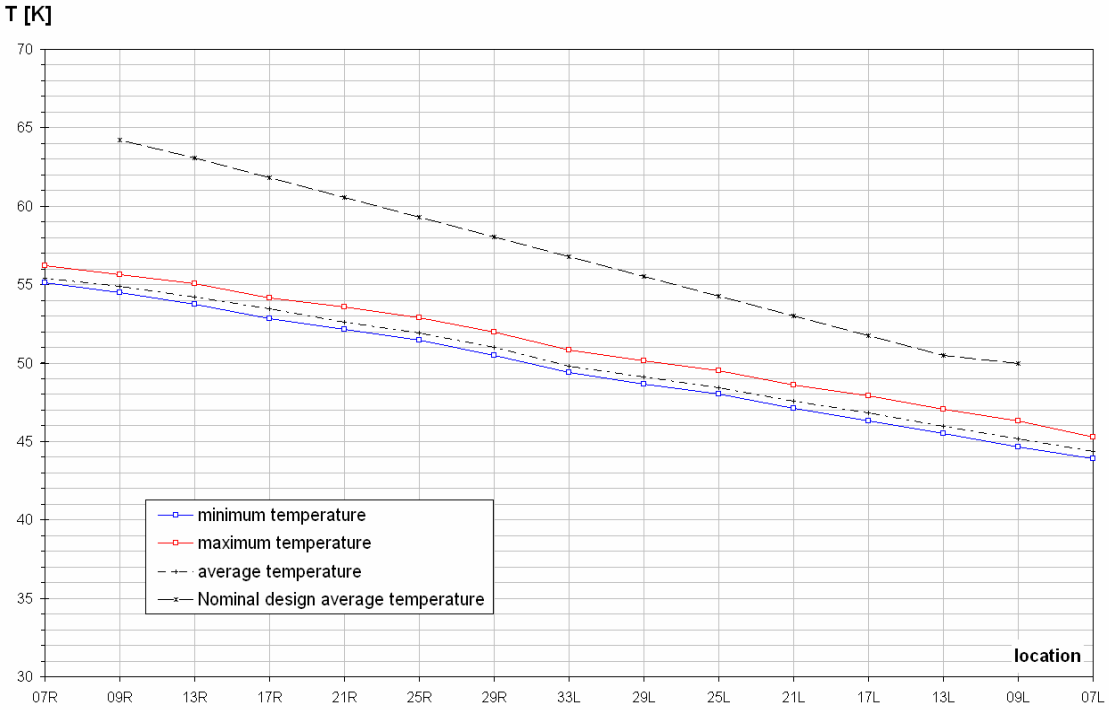

Figure 2 – Line *E* maximum and minimum temperature envelopes and average temperature profiles along sector 7-8, compared to the design profile

2.1 *Header E mass flow*

The method chosen to evaluate the mass flow is based on the overall helium pressure drop Δp inside line *E*, from the first to the last magnets of the sector. Making use of the Darcy-Weisbach equation for hydrodynamic loss due to friction along pipes (see Annex for details), and considering all the different segments *j* that constitutes the header, the mass flow can be evaluated as

$$\dot{m}_E^* = \frac{\pi}{\sqrt{8}} \sqrt{\frac{D^4 \overline{\rho}\, \Delta p}{\sum_{j=1}^{n} 4 f_j \frac{L_j}{D_j}}} \qquad \text{[kg/s]} \qquad (2)$$

where the star indicates that the quantity on the left side of the equation represents a gross mass flow, to be reduced as indicated below. In (2) all quantities are in SI units: f_j, D_j and L_j are the fanning factor, the internal diameter and the overall length of each segment j respectively, while $\overline{\rho}$ is the fluid density averaged along the whole pipe length. Finally, the diameter D represents the most recurrent diameter along the header, and coincides with its nominal diameter.
Header E can be subdivided in different segments, with those mostly affecting the mass flow summarized in Table 2.

Table 2 – Characteristics of header E for mass flow evaluation

#	Segment	Quantity n	Length L [m]	Diameter D [mm]	Fanning factor $4f$	Local resistance ζ
1	Nominal straight pipe	1	3241.5	80	0.0192	-
2	Liner[2]	212	0.479 *(each)*	76.5	0.0747	-
3	Liner – narrowing[3]	212	-	80 to 76.5	-	0.0428
4	"T" junction	7	-	80	-	0.864

Finally, between the two pressure sensors, there are seven "T" junctions in the line, (Figure 3). Each one of them, besides introducing a localized pressure drop already considered in (2), corresponds to an outlet to a dedicated branch for cooling the thermal shield of a stand alone cryomagnet. Hence to calculate the mass flow circulating in the arc cryomagnet only, the value resulting from (2) is reduced by the total outgoing mass flow, giving the *net mass flow*

$$\dot{m}_E = \dot{m}_E^* - \dot{m}_{\sum T} = \dot{m}_E^* - \sum_{j=1}^{6} \dot{m}_j \qquad \text{[kg/s]} \qquad (3)$$

where the mass flow $\dot{m}_j$ for each junction is calculated applying virtual flowmeter[4].

[2] Liner in line E interconnection bellows: there is one liner at each interconnection. The liner was considered as a helically corrugated tube and its fanning factor was calculated as $f_2 = 1.53\left(h_2^2/(p_2 D_2)\right)^{0.46} \mathrm{Re}_D^{-0.16}$ (from Vicente and Garcia, 2003) with h_2 the helical height and p_2 the helical pitch of the helix.

[3] The contraction due to the presence of the liner, as well as the "T" junctions and the elbows, give the equivalence $4 f_j L_j / D_j = n_j \zeta_j$.

[4] To estimate the mass flow, this method makes use of empiric relationships existing between the experimentally determined hydraulic characteristic of a control valve, together with its actual opening and inlet pressure. The overall outgoing mass flow amounts to a small percentage of the total mass flow $\dot{m}_E$.

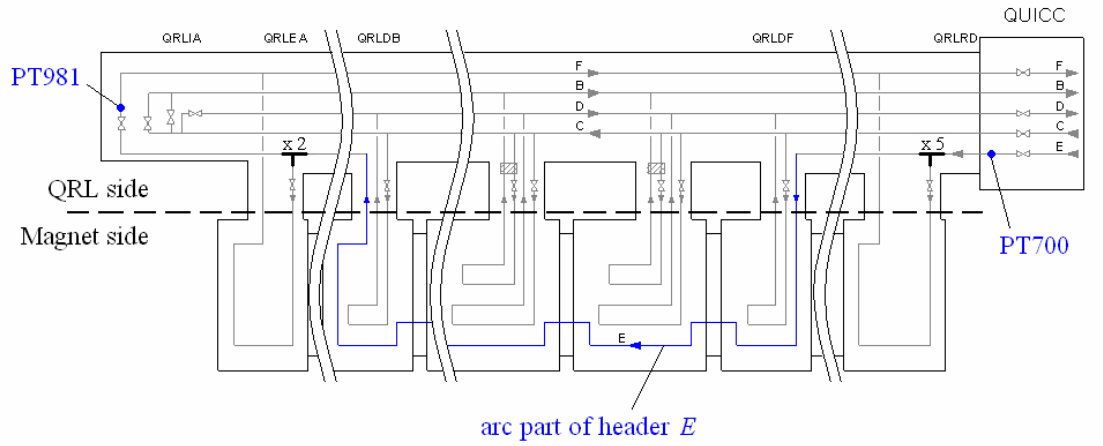

Figure 3 – Cryogenic scheme for the LHC sector 7-8. Between the considered pressure sensors there are five (before the arc) plus two (after the arc) outlets.

2.2 S*tatic heat load*

The heat intercepted by the thermal shield between two subsequent temperature sensors can be evaluated as the enthalpy difference of the coolant between the two sensors, which strongly depends upon the coolant mass flow and average supply temperature T_{supply}. In fact, this temperature does not only affect the overall temperature profile along the cooling line, as said, but also strongly determines the enthalpy levels of heat exchange along the whole line.

The specific enthalpy balance $\Delta h = h_{s+1}(T_{s+1}, p_{s+1}) - h_s(T_s, p_s)$ between the two sensors s and $s+1$ is numerically evaluated with HePAK [2], using temperature and pressure readings, and assuming stationary conditions. But since only two pressure sensors are available within the sector (PT981 and PT700) and since the low value of the overall pressure drop has limited influence on the enthalpy, pressure was assumed constant along the whole line E for enthalpy calculation purposes ($p_s = p_{s+1}$).

The resulting heat load per meter length is then calculated as Δh, calculated at every data acquisition time-step and then averaged over the whole time period, and divided by the distance between two subsequent temperature sensors L_{TT}

$$W_E = \frac{\Delta H_{avg}}{L_{TT}} = \frac{\left(\dot{m}_E \cdot \Delta h\right)_{avg}}{L_{TT}} \qquad \text{[W/m]} \qquad (4)$$

Results are graphically shown in Figure 4, where the computed heat load profile is compared to the expected one: considering only the arc region, the heat load to the thermal shield remains between 3.07 and 4.27 W/m, in average 0.78 W/m lower than the expected load, confirming the good performance of the thermal shielding.

2.2 *Discussion*

The heat load calculation includes three standard deviations for random errors. The error bars become anyway negligible, since the mean heat load W_E is averaged over a sample of 4320 values (one minute acquisition frequency over a period of three days).

It should be kept in mind that the heat load profile is obtained from the enthalpy balance of the coolant, which had a supply temperature lower than the nominal design value. Increasing T_{supply} from the actual to the nominal value, say from 44.6K to 50K, and considering the reasonable hypothesis that ΔT between two generic sensors would

however remain the same as before, the enthalpy balance $\Delta h = \Delta h(\Delta T, T_{supply}, p)$ would slightly decrease. Hence the heat load affecting the thermal shield would decrease further below the calculated profile in full nominal conditions.

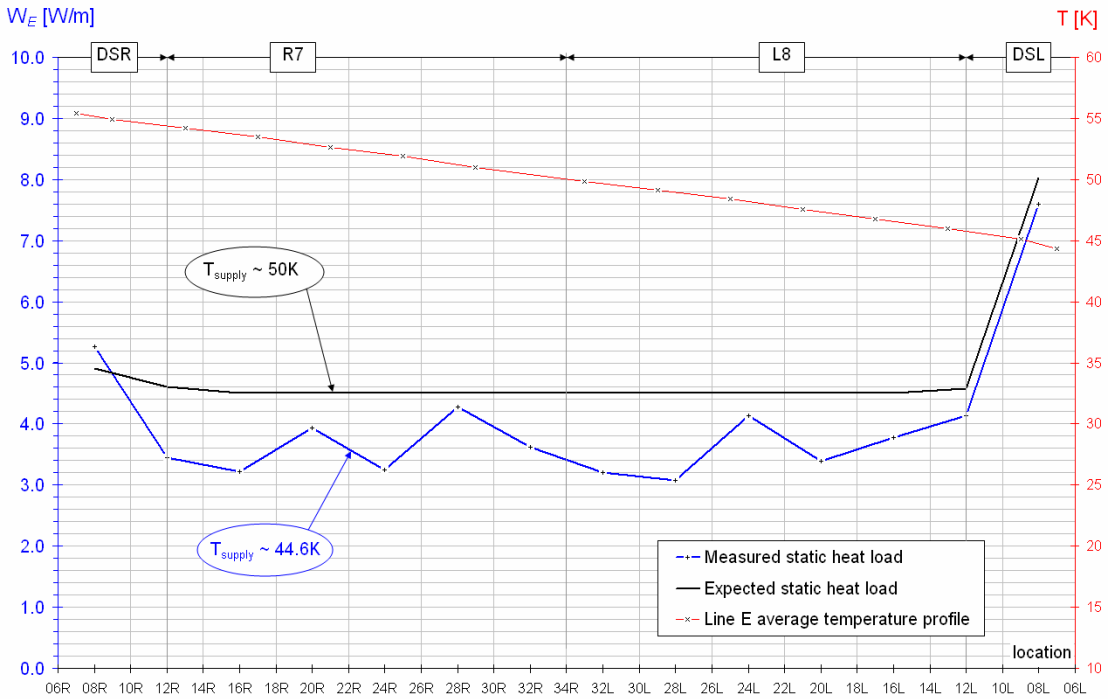

Figure 4 – Thermal shield static heat load profile along sector 7-8

3. COLD MASS STATIC HEAT LOAD

3.1 S*tatic heat load*

The heat load to the cold mass was calculated during a natural warm-up of the sector[5], estimating its overall internal energy variation over time.
In static conditions, the cold mass receives heat from the thermal shield and from various heat intercepts (Figure 1). The heat capacity to be considered is provided by the cold mass constituting materials and by the superfluid helium content of the bath, which has an average value of 25.12 ± 0.47 liter/m, [8]. Since the heat capacity of helium in superfluid state is highly dominant, only its heat capacity has been considered, together with the contribution of steel and copper[6].
As shown schematically in Figure 5, the superfluid helium bath is shared by several cold masses within the same cryogenic subsector and is actively cooled by the saturated helium inside the heat exchanger tubes of each cell.

[5] The warm-up that can be used for a heat load assessment is due to a natural temperature drift of the 1.9K superfluid helium bath. During the first commissioning of sector 7-8, there have been some natural warm-ups due to different issues, but only few of them presented the optimal conditions required for the assessment.
[6] On average, superfluid helium accounts for 98.3% of the total energy variation, Copper only for 0.01% and Steel for the rest.

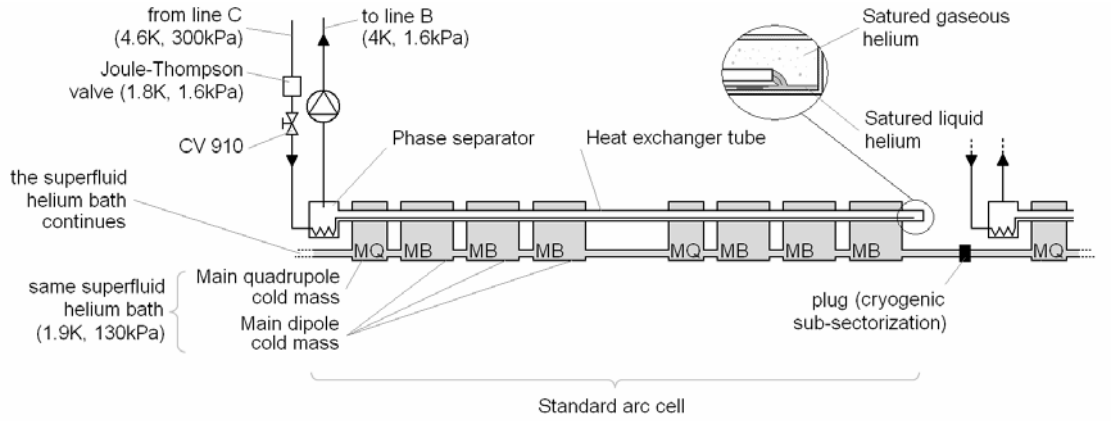

Figure 5 – Schematic cryogenic layout of a standard arc cell. A cryogenic subsector is defined as a unique common superfluid helium bath and includes two or three standard cells. A standard cell includes six dipoles and two quadrupoles and is cooled by a unique heat exchanger tube.

For each cryogenic subsector separately (i.e. for each superfluid helium bath separately), the warm-up starts with the closure of its CV910 valves, which stops the feeding of coolant to the heat exchanger tubes. The time period considered for the calculation starts anyway about twenty minutes later, since the heat exchanger tube needs this time to naturally empty and so to truly stop cooling the cold mass bath, and it ends before helium inside the pressurized bath reaches the lambda temperature[7] (Figure 6).

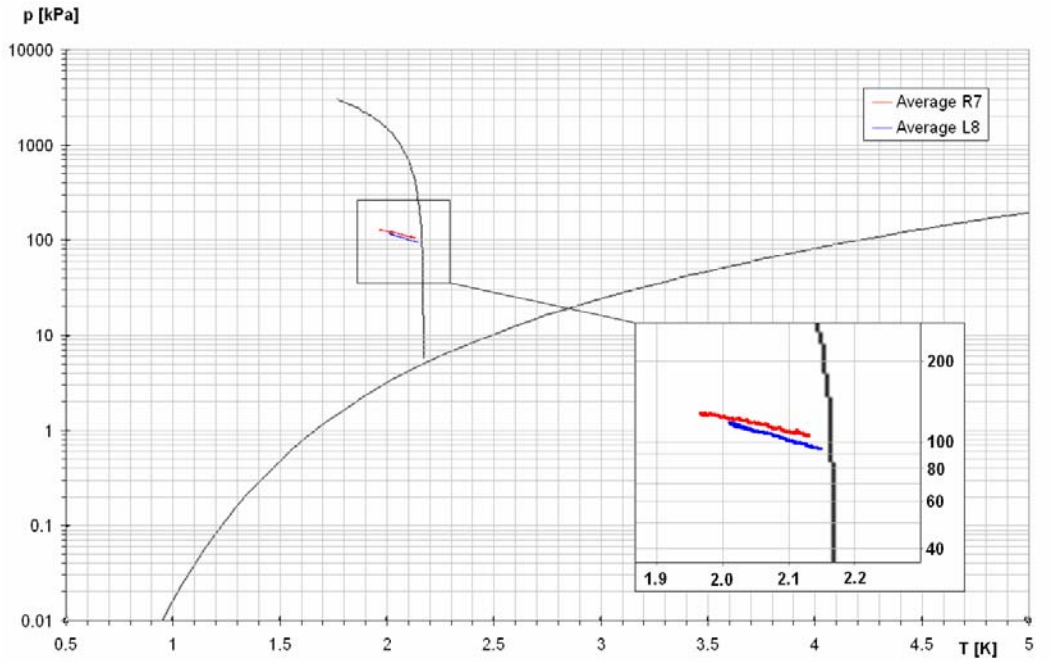

Figure 6 – Average transformation in p-T helium phase diagram for the pressurized superfluid helium in the two halves of the sector.

[7] An additional twenty minutes have to be considered only for natural emptying of the heat exchanger tubes, when pumping from it to line B is stopped (see Figure 5). If pumping continues, the emptying is faster. Moreover, as a condition for the heat load assessment, the temperature has to remain uniform all along the cold mass bath for the entire considered period. But, since there is only one temperature sensor for each 5 to 15m long cold mass, this condition can only be ensured by the extremely large heat transport capacity of pressurized helium in the superfluid state. That is why the time period considered for the assessment must end before helium reaches its normal fluid state (2.15K).

Data were acquired from Timber-SCADA interface, during a period of a few hours, with a one minute acquisition frequency[8]. During this period, line *C'* was maintained in stable nominal conditions, no quench valves were opened and only one event happened in one subsector[9]. Finally, the thermal shield had a supply temperature lower than the nominal one. Sensors used are listed in Table 3.

Table 3 – Sensors for thermal shield heat load evaluation in sector 7-8

Sensor	Reading	Location	Description
CV910	Aperture [%]	One each heat exchanger tube, before the phase separator	Cooling active or not
TT821	T [K]	Approximately one each cold mass	Cold mass temperature
PT821	p [bar]	One each cryogenic subsector	Cold mass pressure

Under these conditions, the heat load per meter length to the cold mass is

$$W_{CM} = \frac{\Delta U_{CM}}{\Delta t \cdot L_{CM}} = \frac{\sum_m \Delta U_m}{\Delta t \cdot L_{CM}} \tag{5}$$

where ΔU_m is the variation of internal energy of the matter (helium, steel or copper), L_{CM} is the cold mass length including interconnections[10] and Δt is the warm-up time period. Results are presented in Figure 7, where the computed heat load profile is compared to the expected one.

[8] For the reasons explained in note 7, the exact time period is different from one cold mass to another, and lasts between 71 and 493 minutes.

[9] If a quench valve of a specific cell in a subsector were opened, the helium content of the entire subsector would not be considered constant anymore, forbidding the heat load estimate for the entire subsector. The event indicated was anyway only an instantaneous (and not better specified) pressure increase, which slightly affected the validity of the analysis for the subsector 11_13R7 only.

[10] Cold mass length includes interconnection length, since the estimated average helium content per m length m_{He} also takes the interconnection length into account.

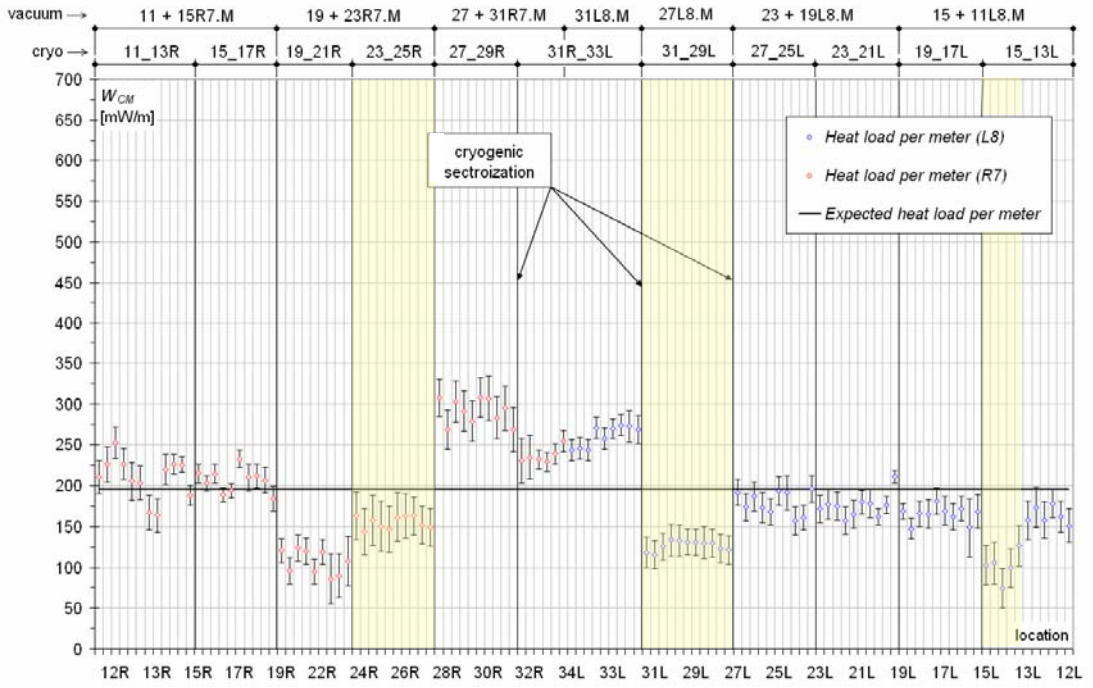

Figure 7 – Cold mass static heat loads in sector 7-8

From the figure, it is clear that cold masses belonging to different cryogenic subsectors behave differently, since different baths are cryogenically independent one from the other. Moreover, apart from the two arc extremities (cryosector 11_13R and 15_13L) and within the error bar uncertainties, all cold masses belonging to the same cryogenic subsector have a similar heat load.

This behavior is a consequence of the high dependence of the heat load upon the superfluid helium bath conditions; as a first approximation, it allows treating entire cryogenic subsectors instead of treating each cold mass separately.

In these terms, Figure 7 shows thermal behavior within specified limits: 64.4% of cold masses have a heat load definitely lower than the expected value, while 73.7% have the error bar minimum value lower than expected. Despite this, for some cryogenic subsectors the heat-load exceeds the expected value, precisely at mid arc (27_29R and 31R_33L) and at far right end of the sector (11_13R and 15_17R). As mentioned previously, for cryo-sector 11_13R, the assessment cannot be considered reliable.

For vacuum sector 31L8, at mid arc, degraded vacuum conditions prevailed[11]; this situation alone could explain the observed excessive heat-load to the entire cryosector 31R_33L, since the common cryogenic bath allows the heat to be diffused over the vacuum sector limit at mid arc.

However, the same vacuum leak cannot be considered responsible for the excessive heat-load affecting the adjacent cryosector 27_29R, since there is a cryogenic sectorization between the two. Therefore heat loads to these cold masses, as well as for cold masses in 15_17R, have to be clarified with further investigations.

3.2 *Discussion*

[11] As the sector has been warmed up, a vacuum leak in cell 33L8 was found. The calculated excess heat-load with respect to the nominal value corresponds to an increase of about an order of magnitude in residual vacuum pressure.

Values in Figure 7 are shown with their error bars. Apart from the random error, the method used for the calculation of the cold mass heat load suffers intrinsically from a systematic error which may influence its accuracy.
As a matter of fact, the warm-up period lasts on average a few hundred minutes, while the average temperature difference is 0.16K, ranging between 0.02K and 0.29K.
The calculation is therefore not reliable for those cold masses with a too small temperature difference, say below 0.1K, where its measured value is comparable to that of the sensor accuracy (0.01K at 1.6-2.2K): from this view-point only 67.8% of the cold masses upheld the conditions for a reliable calculation. Data shows that cryosector 27_29R falls clearly within this percentage, having an average temperature gap of 0.19K. Cold masses which do not satisfy this condition are yellow-painted in Figure 7.
Moreover, another systematic error arises from the measurement, this time due to the acquisition system. Even if the acquisition frequency (one reading per minute) leads finally to an acceptable error bar dimension, the acquisition system itself (TIMBER) has an unacceptable filtering action which, within this average temperature gap, turned out few (less than ten) actual values[12] for each cold mass [6] [7]. This filter therefore renders absolutely ineffective the chosen acquisition frequency.
Finally, it is important to remember that the thermal shield, during the warm-up, had a supply temperature which was still lower than the nominal value. While an increase in this temperature would decrease the heat load to the thermal shield, as noticed, on the other hand it would increase the heat load to the cold mass, since both conductive and radiative heat transfer mechanisms between the thermal shield and the cold mass would increase their magnitudes.
All these aspects lead to the conclusion that the heat load diagram of Figure 7 slightly underestimates the *nominal* static heat load to the cold mass.

4. CONCLUSIONS

The heat load assessment has been carried out for thermal shield and cold masses in the LHC arc of sector 7-8, taking advantage of the opportunity offered by its first commissioning in spring/summer 2007.
Results generally show a good agreement with design estimates. Moreover, extrapolation of the values measured from off-nominal supply temperature of the thermal shield to nominal conditions yields heat loads for the thermal shield somewhat lower than the design value. But as a consequence, heat load to the cold masses would increase, as compared to that measured, but hopefully would remain within the design value.
Some uncertainties still remain regarding the cold masses, due both to the data acquisition system and to the warm-up method for calculating the heat load. In this regard a much higher sampling frequency without a filtering action would be advisable for the analysis of the other sectors.

5. REFERENCES

[1] M. Castoldi, M. Pangallo, V. Parma, G. Vandoni, *Thermal Performance of the Supporting System for the Large Hadron collider (LHC) superconducting Magnets*, LHC Project Report 335, CERN, Geneva 1999.
[2] Cryodata Inc., *User's Guide to HEPAK Version 3.4*, Cryodata Inc, USA 1999.

[12] For all the other readings the system copies backward the actual value, sometimes for several minutes, since the filter prevent it to feel any change from the sensor reading.

[3] L. Tavian, T. Durand, A. Ballarino, C. fischer, A. Hilaire, B. Jeanneret, B. Jenninger, R. Ostojic, J.L. Perinet-Marquet, J.P. Tock, A. Poncet, G. Riddone, V. Rodel, F. Ruggiero, D. Brandt, P. Sacre, A. Perin, U. Wagner, R. Van Weelderen, *Heat Load Assessment*, http://lhc-mgt-hlwg.web.cern.ch/lhc-mgt-hlwg/ , CERN, Geneve 2001.
[4] J.B. Bergot, N. Bourcey, L. Nielsen, V. Parma, P. Rohmig, E. Roy, *thermal Performance of the LHC short Straight Section Cryostat*, LHC Project Report 571, CERN, Geneva 2002.
[5] N. Bourcey, O. Capatina, V. Parma, A. Poncet, P. Rohmig, L. Serio, B. Skoczen, J.P. Tock, L.R. Williams, *Final Design and Experimental Validation of the Thermal Performance of the LHC Lattice Cryostats*, LHC Project report 689, CERN, Geneva 2004.
[6] EDMS Document n. 850853: *Minutes*, from the Cryogenic Performance Panel Meeting of May 4, 2007 (Point 8 on page 3).
[7] EDMS Document n. 859329 v.1: *Understanding Cryogenics LHC Logging Data*, from the Cryogenic Performance Panel Meeting of June 12, 2007.
[8] C. Maglioni, V. Parma, *Assessment of Average Helium Quantity per Unit Length of LHC Arc Cold Masses*, LHC Note **XXX**, CERN, Geneva 2007.

6 ANNEX

6.1 *Mass flow evaluation method*

Header *E* mass flow has been evaluated using the Darcy-Weisbach formula, which is generally used for calculating the pressure drop due to distributed resistances along pipes. It states:

$$\Delta p = 4 f \frac{L}{D} \frac{\overline{\rho}}{2} U^2 \tag{6}$$

where Δp is the pressure drop to be evaluated, f the pipe fanning factor, D and L respectively the pipe internal diameter and overall length, $\overline{\rho}$ the fluid average density along the pipe length and U the fluid velocity, averaged over the pipe cross section. In case of a multiple pipe, or if the pipe has different segments j with different characteristics f_j, L_j and D_j, the overall pressure drop results from the sum of single pressure drops at each segment:

$$\Delta p = \sum_{j=1}^{n} \Delta p_j = \sum_{j=1}^{n} 4 f_j \frac{L_j}{D_j} \frac{\overline{\rho}}{2} \overline{U}^2 \tag{7}$$

approximating the average density of the fluid $\overline{\rho}$ and its average velocity U as independent from the considered segment ($\overline{\rho}_j = \overline{\rho}$ and $U_j = \overline{U}\ \forall j$).
In the case where the overall pressure drop is known from measurements, mass flow in the pipe can be estimated reversing (2) to calculate the average velocity $\overline{U}$:

$$\overline{U} = \sqrt{\frac{2\Delta p}{\sum_{j=1}^{n} 4 f_j \frac{L_j}{D_j} \overline{\rho}}} \tag{8}$$

from which equation (2) can be developed using:

$$\dot{m}_E^* = \pi \frac{D^2}{4} \overline{\rho} \overline{U} \tag{9}$$

It has to be noted, however, that $4f_j$ depends upon the pipe roughness and upon the Reynolds number Re_D, as from the Moody diagram, where:

$$\mathrm{Re}_D = \frac{\overline{U} D}{\nu} \tag{10}$$

with ν the kinematic viscosity of the fluid. Hence $4 f_j = 4 f_j\left(\overline{U}\right)$ and mass flow $\dot{m}_E^*$ cannot be calculated directly with (2). Instead, it is calculated with the average velocity $\overline{U}_F$ that finally results from an iterative loop. This loop firstly evaluates the average velocity $\overline{U}_i$ from (8) by assuming a starting value of the fanning factor, then it calculates the corresponding Reynolds number, enters the Moody diagram, calculates the new fanning factor and re-calculates the velocity $\overline{U}_{i+1}$. The loop continues until the two calculated values $\overline{U}_i$ and $\overline{U}_{i+1}$ are close enough one to the other.

Finally the diameter *D*, which appears in equations (2), (9) and (10) is the diameter which mostly affects velocity, density and Reynolds number. It is the most recurrent diameter along the line, which is the nominal one[13]. This, together with the approximations on $\overline{\rho}$ and $\overline{U}$, make the iterative process much easier.

6.2 *Internal energy variations for helium, steel and copper*

For copper and steel, the variation of internal energy is

$$\Delta U_{Cu,St} = \int_{Ti}^{Tf} m_{Cu,St} \cdot C_{P\ Cu,St}(T)\, dT \tag{11}$$

where *m* is the mass, $C_P(T)$ the specific heat capacity at constant pressure[14] while T_i and T_f are the initial and final temperatures, considered to be the same as those of superfluid helium. For the latter, the variation of internal energy is

$$\Delta U_{He} = m_{He} \cdot \Delta u_{He}(T, p) \tag{12}$$

where m_{He} is the estimated average helium content of the cold mass bath [8] and Δu_{He} is the variation of helium specific internal energy, numerically calculated with HePAK [2] as a function of pressure and temperature[15].

[13] Making this approximation means neglecting the direct influence of different segments on the value of mass flow and Reynolds number, leaving their influence only on the overall distributed resistance by means of their weights in denominator of equation (2). As a matter of fact, and luckily enough, header *E* is an almost straight pipe with a little length percentage of low-influence segments, leaving the nominal diameter to be the one which mostly affects velocity, density and Reynolds number.

[14] Specific heat capacity at constant pressure for the two materials is calculated using Debye functions approximated for low temperature.

[15] Rigorously, if helium density is verified to be constant during the entire warm-up as done here, the pressure variation is a consequence of temperature increase due to the heat load. Therefore, internal energy variation should be expressed as function of the solely temperature $\Delta u_{He} = \Delta u_{He}(T)$. This means that beginning from anywhere in the superfluid state of the helium phase diagram, the warming-up transformation at constant density is always prefixed. But, while this is true for variations, the starting (or ending) pressure level of the transformation is anyway necessary to individuate the transformation starting point. Hence, the use of actual pressure values in equation (10) is redundant from a physical point of view, but anyway necessary as a software input.